



Exergy analysis of direct-expansion solar-assisted heat pumps working with R22 and R433A

L. Paradeshi¹ · M. Mohanraj² · M. Srinivas¹ · S. Jayaraj¹

Received: 27 November 2017 / Accepted: 25 May 2018 / Published online: 13 June 2018
© Akadémiai Kiadó, Budapest, Hungary 2018, corrected publication September/2018

Abstract

In this paper, the exergy performance of direct-expansion solar-assisted heat pump systems working with R22 and R433A (mixture of R290 and R1270, 70:30 by mass) was experimentally assessed. The experiments were carried out under the metrological conditions of Calicut in India. (Longitude and latitude of location are 75.78°E and 11.25°N, respectively.) The artificial neural network model was developed for simulating the performance of a direct-expansion solar-assisted heat pump system to have realistic performance comparison. The experimental data observed during the year 2016 were used for training and testing the performance of network. The results showed that the network predicted exergy performance of a direct-expansion solar-assisted heat pump was found to be closer to the experimental results with a maximum fraction of absolute variance, minimum root-mean-square values and coefficient of variance. The system exergy destruction of R22 and R433A was found to be 1.36 and 1.25 kW, respectively. Moreover, R433A is identified as an energy-efficient and environmental-friendly alternative to phase out R22 in solar-assisted heat pump systems.

Keywords Direct-expansion solar-assisted heat pumps · R433A · Exergy performance

List of symbols

A	Area of collector (m^2)
ANN	Artificial neural network
COV	Coefficient of variance
\dot{E}_x	Exergy rate (kW)
E_x	Specific exergy (kJ kg^{-1})
GWP	Global warming potential
h	Enthalpy (kJ^{-1})
I	Irreversibility(kW)
I_t	Total solar insolation (W m^2)
\dot{m}	Mass flow rate (kg s^{-1})
MLFFN	Multilayer feed-forward network
N	Speed of the compressor (RPM)
ODP	Ozone depletion potential
R^2	Fraction of absolute variance
RMSE	Root-mean-square error
S	Entropy ($\text{kJ kg}^{-1} \text{K}^{-1}$)
T	Temperature ($^{\circ}\text{C}$)

\dot{W} Work input rate (kW)

Subscripts

a	Air
amb	Ambient
con	Condenser
dest	Destruction
e	Evaporator
eff	Efficiency
ele	Electrical
i	Component in the system
in	Inlet
Mech	Mechanical
out	Outlet
r	Refrigerant
rad	Radiation
s	Sky
vol	Volumetric
0	Reference/dead state

✉ L. Paradeshi
lokeshpb@gmail.com

¹ Department of Mechanical Engineering, National Institute of Technology, Calicut, India

² Department of Mechanical Engineering, Hindusthan College of Engineering and Technology, Coimbatore, India

Greek symbols

Δ	Change
ε	Exergy efficiency
η	Mechanical efficiency

Introduction

Heat pumps are identified as energy-efficient devices due to its ability to deliver more heat output than the electricity input it takes [1]. Heat pumps are widely employed for heating applications such as drying [2], water heating [3], space heating and desalination [4]. The performance of the heat pump systems is improved by integrating the system with renewable sources such as solar [1–4], geothermal [5] and its hybrid form [6, 7]. Out of these options, solar energy is an ideal and economical choice. Hence, lots of research and developments have been made with direct-expansion solar-assisted heat pump (DXSAHP) systems during last decade [8]. Most of the solar-assisted heat pump systems reported in the literature were using halogenated refrigerants due to its good thermodynamic and thermo-physical properties [9]. However, such halogenated refrigerants have poor environment properties concerning ozone depletion potential and global warming potential.

Recent Paris environmental protocol 2016 restricted the use of halogenated refrigerants in refrigeration, air-conditioning and heat pump systems. More than 198 countries including India have agreed to reduce the consumption of halogenated refrigerants. Hence, it is essential to look for energy-efficient and environmental-friendly alternative refrigerants to replace the existing halogenated refrigerants. Many research and development studies reported in the open literature confirmed that hydrocarbon refrigerants are energy-efficient and environment-friendly alternatives to phase out existing halogenated refrigerants in refrigeration, air-conditioning and heat pump systems [10–12]. However, the flammability risks of hydrocarbon refrigerants restrict the usage of existing systems. Hence, some safety mechanism needs to be made while retrofitting with hydrocarbon refrigerants. Moreover, it is essential to identify the inefficient components in the system while retrofitting with hydrocarbon refrigerants.

Exergy analysis based on second law of thermodynamics is a valuable tool for identifying the inefficient components in the heat pump systems [3]. In a related work, Mohanraj et al. [13] assessed the exergy performance of a DXSAHP system using R22 and its alternatives (mixture of R407C and LPG). It was reported that the evaporator–collector was identified as the major inefficient component in the system. In a similar work, Hepbasli [14] assessed the exergy performance of a solar-geothermal hybrid source heat pump system using R410A. It was concluded that the system exergy destruction and exergy efficiency were found to be 3.39 kW and 72.33%, respectively. Similarly, many research investigations have been reported on exergy analysis of DXSAHP systems and identified the

compressor and evaporator–collector as major inefficient components in the system [15–23].

The performance simulation of DXSAHP systems under different ambient conditions is essential to have realistic performance comparison, while the system is working with two different refrigerants. Earlier research investigations confirmed that artificial neural networks were successfully used for performance prediction of refrigeration, air-conditioning and heat pump systems [24], energy systems [25] and heat exchangers [26]. The artificial neural network model was successfully used for predicting the energy performance of DXSAHP systems [27]. Their results reported that the multilayer feed-forward network model with 2-10-4 predicts the energy performance of the heat pump with maximum fraction of absolute variance of 0.9999 and minimum root-mean-square error and minimum coefficient of variance. Similarly, the coefficient of performance of a geothermal heat pump system was predicted using multilayer feed-forward network model [28]. It was reported that 3-7-1 configuration predicts the coefficient of performance with good statistical performance values. In another work, the photovoltaic thermal hybrid evaporator of a heat pump was modeled using multilayer feed-forward network [29]. It was reported that 4-15-4 configuration predicts the performance of a heat pump with good prediction accuracy.

From the cited literature, it is understood that there is specific research work has been reported on the use of R433A mixture in DXSAHP systems as drop in substitute. Hence, an attempt has been made in this research work to identify the inefficient components in the R22-based DXSAHP systems while retrofitted with R433A mixture. Two multilayer feed-forward networks have been developed for simulating the exergy performance of a DXSAHP system to have realistic performance comparison.

Experimental

The experiments were carried out in the year 2016 during January to April, at Calicut located in southwest coasted region of India.

Experimental of setup

The schematic layout of the experimental setup is illustrated in Fig. 1, and its technical specifications are given in Table 1. The system consists of basic components such as a hermetically sealed compressor (with 1020 W rated power input), finned tube air cooled condenser, thermostatic expansion valve and an evaporator–collector (with 2 m² area). The evaporator–collector has thermosyphon arrangement having 25 mm header at the top side and

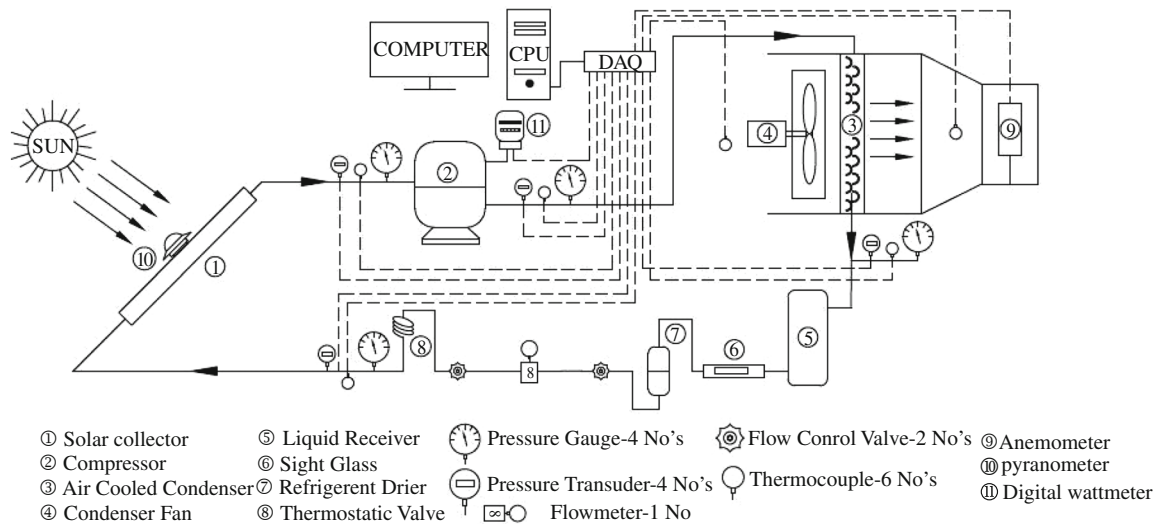


Fig. 1 Schematic representation of DXSAHP system

Table 1 Specification of various components used in the DXSAHP system

Component	Specification
Compressor	Rated power input 1020 W; Cooling capacity 2750 W; Speed: 2800 rpm;
Condenser	Air cooled condenser with 9.52 mm dia; Air velocity; through duct: 4.8 m s ⁻¹ , Tube material Copper
Expansion device	Thermostatic expansion valve
Collector-Evaporator	Glazed solar collector of area 2 m ² with 0.8 mm thick copper fins as absorber surface
Refrigerant	R22, R433A

bottom side connected by eight numbers of 9.5-mm tubes. The plate fins are brazed with the tubes to increase the absorption area. The fins and tubes are coated with black paint to enhance the rate of absorption, which is placed behind the gazing surface by maintaining 25 mm gap to generate greenhouse effect. Moreover, the presence of glazing reduced the convective and radiative losses from the absorber plate. The bottom side of the absorber plate is insulated with 20 mm thickness of glass wool to reduce the heat loss from the lower side of the evaporator collector. Accessories such as liquid receiver and sight glass are fitted in the liquid line. The sealed-type refrigerant drier was installed at the condenser outlet to absorb the moisture present in the working fluid. The evaporator–collector is tilted at an angle of 20° facing toward south to maximize the rate of heat absorption [30].

Measurements

The refrigerant circuit of the heat pump system is equipped with four Bourdon tube pressure gauges and four pressure transducers (at compressor inlet and outlet and expansion valve inlet and outlet) to observe the respective refrigerant

pressures in the heat pump circuit. In addition, four PT-100 thermocouples with an accuracy of ± 0.2 °C were installed for measuring the refrigerant temperatures at respective points in the heat pump circuit. In addition, two thermocouples with same specification were installed at condenser entry and exit for measurement of air temperature. All the pressure transducers and thermocouples were interfaced with a computer through a data logger. The solar irradiation that falls on the evaporator–collector was measured using a pyranometer with the accuracy of ± 5 W m⁻². The ambient temperature is measured using a precision thermometer with ± 0.5 °C. The airflow mass flow rate through the condenser was measured using an orifice manometer setup fitted at the condenser outlet. The compressor power consumption was measured using a Wattmeter. The technical details of the measuring instruments are listed in Table 2.

Experimental procedure

The system was initially flushed and leak-tested with nitrogen gas to remove the impurities inside the system. The air and non-condensable gases were removed with the

Table 2 Specification of measuring instruments used in experimental setup

Instrumentation	Specification/range	Accuracy
Temperature sensor	PT 100/0–200 °C	± 0.2 °C
Pressure sensor	HAE-24/0–24 bar	± 0.01 bar
Thermometer	0–100 °C	± 0.5 °C
Anemometer	Vane type	± 0.1 m s ⁻¹
Pyranometer	Class A, 0–1500 W m ⁻²	± 5 W m ⁻²
Wattmeter	Digital type	± 1 W

help of a vacuum pump. The system was charged with 1100 g of R22 according to the manufacturer specifications. The system was turned ON and allowed to run for the period of one hour to attain steady-state conditions and to avoid initial transient errors. The system operating parameters (such as pressure and temperature of refrigerant at typical locations of heat pump circuit, air temperatures at the condenser inlet and outlet) and ambient parameters (such as solar irradiation, ambient temperature and ambient wind velocity) were measured every ten minutes interval from 9.00 to 18.00 h. The experimental observations were recorded in the computer at every one-minute interval to investigate the transient behavior of the system. After completion of baseline test with R22, the refrigerant was recovered from the heat pump and the equivalent amount (450 g) of R433A mixture was charged in the system. The equivalent quantity of R433A was obtained based on liquid density values noted from the REFPROP® database. The experimental procedure was repeated for R433A mixture.

Uncertainty analysis

The uncertainties associated with performance assessments were due to the accuracy of measuring instruments [15, 16]. The uncertainties are calculated using the following relation:

$$u_f = \left[\left(\frac{\partial f}{\partial x_1} u_{x_1} \right)^2 + \left(\frac{\partial f}{\partial x_2} u_{x_2} \right)^2 + \dots + \left(\frac{\partial f}{\partial x_n} u_{x_n} \right)^2 \right]^{1/2} \tag{1}$$

The uncertainties in exergy destruction and exergy efficiencies of the compressor, condenser, expansion valve, collector–evaporator and total system are found to be ± 2.14, ± 1.42, ± 1.98, ± 2.9 and ± 4.6%, respectively.

Exergy analysis

The maximum work potential of a system with respect to the ambient conditions (dead state) is called exergy. The exergy assessment of heat pump systems is essential to quantify the energy losses and to identify the inefficient components. The general form of the exergy balance equation is represented by:

$$\sum \dot{E}x_{dest} = \dot{E}x_{in} - \dot{E}x_{out} \tag{2}$$

The exergy balance of DXSAHP system is given by:

$$\dot{E}x_{rad} + \dot{W}_{comp} = \dot{E}x_{con} + \sum \dot{i}_{ir} \tag{3}$$

The specific exergy and exergy change rate at typical location in a DXSAHP circuit is given by following equations:

$$e_x = (h - h_0) - T_0(s - s_0) \tag{4}$$

$$\dot{E}x = \dot{m}e_x \tag{5}$$

The DXSAHP system consists of a compressor, condenser, expansion valve and collector–evaporator. The pressure–enthalpy diagram of a DXSAHP system is depicted in Fig. 2. The thermodynamic states of the DXSAHP system are represented at compressor inlet, compressor outlet, condenser outlet and expansion valve outlet by state points 1, 2, 3 and 4, respectively. Here, 1–2 indicates the compression, 2–3 indicates condensation, 3–4 indicates expansion, and 4–1 indicates evaporation. Processes 1–1' and 3–3' gives super heating and sub-cooling, respectively. Air temperature at the condenser inlet and outlet is represented by 5 and 6, respectively.

The exergy analysis of a DXSAHP system and its components is performed with the following assumptions:

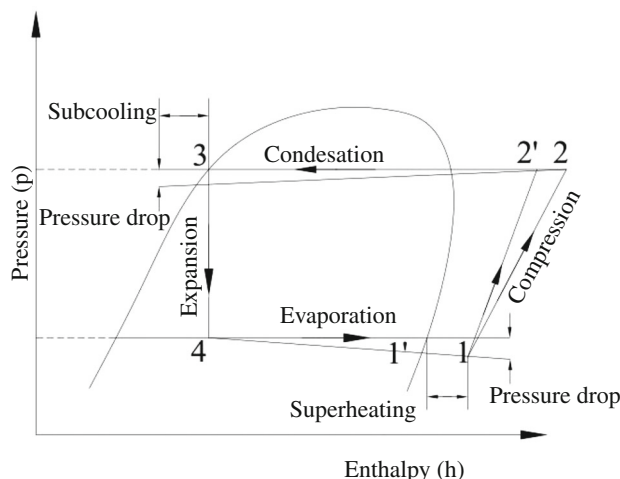


Fig. 2 p–h diagram of a DXSAHP system

1. All processes are corresponding to the steady-state conditions.
2. Kinetic and the potential exergy terms are neglected.
3. Compressor speed and stroke are assumed constant. (2800 RPM and $18.27 \text{ cm}^3 \text{ rev}^{-1}$, respectively.)
4. Convective and radiation losses in the evaporator–collector are ignored.
5. Atmospheric pressure (101.103 kPa) and temperature ($25 \text{ }^\circ\text{C}$) conditions are considered corresponding to the dead state (reference state).

Compressor

The exergy destruction and exergy efficiency of the compressor are determined using the following relations:

$$\dot{E}x_{\text{dest,comp}} = \dot{E}x_1 - \dot{E}x_2 + \dot{W}_{\text{comp}} \quad (6)$$

$$\varepsilon_{\text{comp}} = \frac{\dot{E}x_1 - \dot{E}x_2}{\dot{W}_{\text{comp}}} \quad (7)$$

Here \dot{W}_{comp} is the work input to the compressor (W). The compressor work is given by:

$$\dot{W}_{\text{comp}} = \frac{\dot{m}_r(h_2 - h_1)}{\eta_{\text{mech}} \times \eta_{\text{ele}}} \quad (8)$$

where \dot{m}_r is the mass flow rate of the refrigerant (kg s^{-1}), h_1 and h_2 are enthalpy of refrigerant at inlet and outlet of the compressor, respectively ($\text{kJ kg}^{-1} \text{ K}^{-1}$). The mechanical and electrical efficiency of the compressor is assumed as 0.75 and 0.75, respectively.

The refrigerant mass flow rate is given by:

$$\dot{m}_r = \frac{V_{\text{disp}} \eta_{\text{vol}} N}{60 v_1} \quad (9)$$

where V_{disp} is the volumetric displacement ($\text{cm}^3 \text{ rev}^{-1}$) and v_1 is the specific volume of the refrigerant ($\text{m}^3 \text{ kg}^{-1}$).

Condenser

The condenser exergy destruction and exergy efficiency are calculated using the following relations:

$$\dot{E}x_{\text{dest,cond}} = (\dot{E}x_2 - \dot{E}x_3) + (\dot{E}x_6 - \dot{E}x_5) \quad (10)$$

$$\varepsilon_{\text{cond}} = \frac{\dot{m}_a(\dot{E}x_6 - \dot{E}x_5)}{\dot{m}_r(\dot{E}x_2 - \dot{E}x_3)} \quad (11)$$

where \dot{m}_a is the mass flow of air (kg s^{-1}). It is experimentally measured as 0.0228 kg s^{-1} . The total exergy rates $\dot{E}x_5$ and $\dot{E}x_6$ are calculated using the temperature of the air at inlet (T_5) and outlet (T_6) of the condenser, respectively.

Expansion valve

The exergy destruction and exergy efficiency of an expansion device are given by the following equations:

$$\dot{E}x_{\text{dest,txv}} = \dot{E}x_3 - \dot{E}x_4 \quad (12)$$

$$\varepsilon_{\text{txv}} = 1 - \left(\frac{\dot{E}x_{\text{dest,txv}}}{\dot{E}x_{\text{in}}} \right) \quad (13)$$

Evaporator–collector

The following relations were proposed by Kara et al. [21] to calculate the exergy destruction and exergy efficiency of an evaporator–collector:

$$\dot{E}x_{\text{dest,sol.coll}} = \dot{E}x_{\text{collected}} - \dot{E}x_{\text{used}} \quad (14)$$

$$\varepsilon_{\text{sol.coll}} = \frac{\dot{E}x_{\text{collected}}}{\dot{E}x_{\text{used}}} \quad (15)$$

Equations (16) and (17) were used to calculate the exergy collected and exergy used in the solar collector, respectively [22].

$$\dot{E}x_{\text{used}} = \left[\dot{m}_r(h_{r,\text{out}} - h_{r,\text{in}}) \frac{T_0 - T_e}{T_e} \right] \quad (16)$$

$$\dot{E}x_{\text{collected}} = A I_t \left[1 + \frac{1}{3} \left(\frac{T_0}{T_{\text{sr}}} \right)^4 - \frac{4}{3} \left(\frac{T_0}{T_s} \right) \right] \quad (17)$$

where $h_{r,\text{in}}$ and $h_{r,\text{out}}$ are enthalpy of the refrigerant at inlet and outlet of the evaporator–collector ($\text{kJ kg}^{-1} \text{ K}^{-1}$), respectively.

Total system

The system exergy destruction is the sum of exergy destruction in all the system components (compressor, condenser, expansion valve and evaporator–collector). The total exergy destruction and system exergy efficiency of a DXSAHP system are given by following relations:

$$\dot{E}x_{\text{dest,system}} = \dot{E}x_{\text{dest,comp}} + \dot{E}x_{\text{dest,cond}} + \dot{E}x_{\text{dest,txv}} + \dot{E}x_{\text{dest,sol.coll}} \quad (18)$$

$$\varepsilon_{\text{system}} = 1 - \left(\frac{\dot{E}x_{\text{dest}}}{\dot{E}x_{\text{in}}} \right) \quad (19)$$

Characteristics of R22 and R290/R1270 mixture

The R433A is a binary mixture composed of R290/R1270 (in the ratio of 70:30, by mass) identified as a possible alternative to phase out R22 in refrigeration, air-conditioning and heat pump systems. The properties of mixtures obtained from REFPROP 9.0[®] database have been used in this work. The thermo-physical, thermodynamic and environmental properties of R22 and R433A are described in this section.

Thermo-physical properties such as vapor pressure and latent heat of R22 and R433A in the temperature ranging between 0 and 70 °C are illustrated in Figs. 3 and 4, respectively. It is observed that the vapor pressure of R433A is found to be closer to R22 in the temperature range between 0 and 40 °C. At higher temperatures, the vapor pressure of R433A is found to be lower when compared to R22 by about 3.8%, which confirms that compressor power consumption would be less when compared to R22. From Fig. 4, it is noticed that the latent heat of R433A is about 108% higher when compared to R22 for the given temperature range. The refrigerant R433A is capable of absorbing more heat through the evaporator-collector due to its higher latent heat when compared to R22 across a wide range of operating temperatures.

Similarly, the liquid density of R22 and R433A in the temperature range between 0 and 70 °C is compared in Fig. 5. The R433A is having 58% lower density (average value) when compared to R22 in the temperature ranges between 0 °C and 70 °C. Hence, the R433A mass charge requirement would be lower than that of R22 by about 50%. The theoretical compression ratio of R22 and R433A is depicted in Fig. 6. The compressor pressure ratio for the

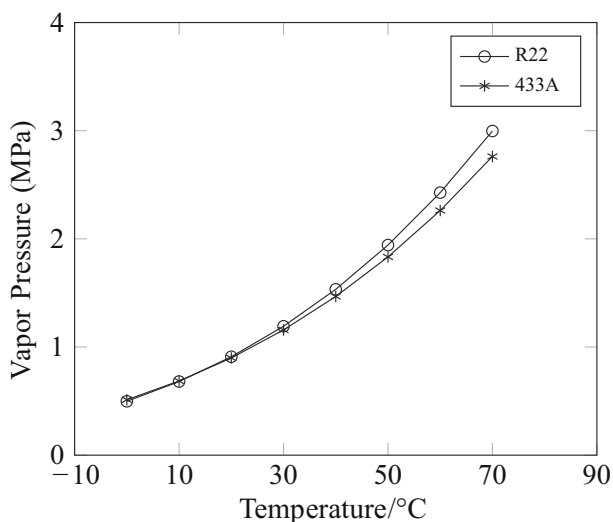


Fig. 3 Saturation pressure versus temperature

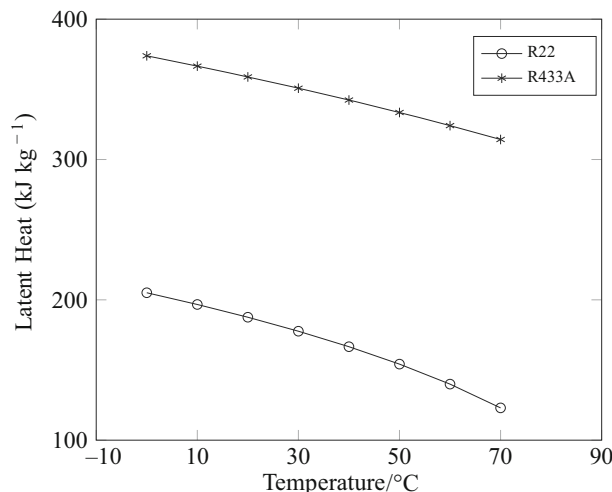


Fig. 4 Latent heat versus temperature

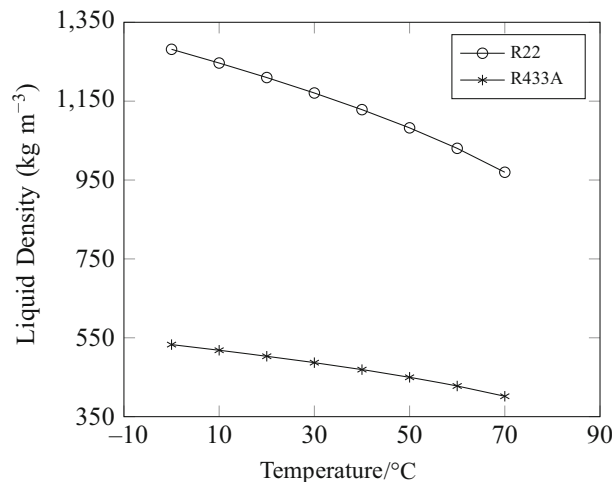


Fig. 5 Liquid density versus temperature

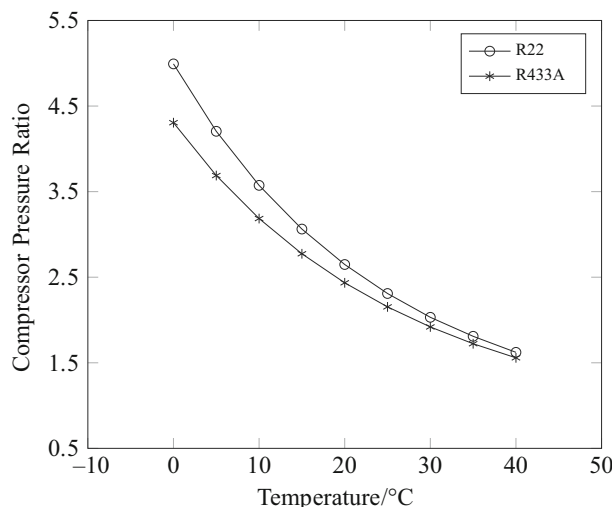


Fig. 6 Variation of pressure ratio

R433A is found to be slightly lower when compared to R22. The lower compressor pressure ratio of R433A results improvement of compressor volumetric efficiency and also reduces the compressor power consumption.

The thermodynamic and environmental properties of R22 and R433A are listed Table 3. The critical pressure of R433A is found to be closer to R22. The critical temperature of R433A is found to be slightly lower when compared to R22. The ozone depletion potential (ODP) of R433A mixture is found to be zero with low global warming potential (GWP) compared to that of R22. Moreover, the R433A is miscible with the mineral oil, which is used in the existing R22 systems. Hence, they can be directly used as an alternative to the available R22 systems. The R433A is a suitable alternative to R22 for vapor compression-based refrigeration, air-conditioning and heat pump systems.

Exergy performance simulation using artificial neural networks

The performance simulation of a DXSAHP system for different ambient conditions is essential to have realistic performance comparison when the system is working with two different working fluids. Two multilayer feed-forward networks with two neurons in input layer (representing solar irradiation and ambient temperature) and five neurons in output layer representing exergy destruction (of each components compressor, condenser, expansion valve, evaporator–collector and for the whole system) and exergy efficiency were considered. The configuration of multilayer feed-forward network with its names of inputs and outputs is schematically illustrated in Figs. 7 and 8, respectively. The experimentally observed data were used for training and testing the performance of the network. The 75% of the experimental data were used for training the multilayer feed-forward network, and the remaining 25% of experimental data were used to validate the network performance.

In order to train the network, ‘trainlm’ function was used. This type of network training function updates weight

and bias values according to the ‘Levenberg-Marquardt’ optimization method. ‘Learnngdm’ is used for adoption learning function. It is the gradient descent with momentum weight and bias learning function. As suggested by Mohanraj et al. [13, 20], the number of hidden neurons is calculated using the formula proposed by Bechtler et al. [31].

$$h_n = \frac{1}{2} + (i_a + i_b) + \sqrt{i_c} \quad (20)$$

where h_n is the number of hidden neurons, i_a and i_b are a number of input and outputs and i_c is the number of training data used. The input signal of a neuron is made to pass the output signal using the logistic function. The logistic sigmoid transfer is given by the following equation.

$$f(z) = \frac{1}{1 + e^{-z}} \quad (21)$$

The variable z in the above equation is given by:

$$z = f \left[\sum_i w_i x_i \right] \quad (22)$$

where z is the weighted input, i is the index on the inputs to the neurons, x_i is the input to the neuron, and w_i is the weighted factor attached to that of input. After changing all these options, a neural network structure is formed. Three variants (namely the statistical values of root mean square, coefficient of variance and fraction of absolute variance, which gives a minimum error) are chosen for the performance prediction of the DXSAHP system. These parameter values will confirm how well the input and output data are fitted in the network. While it indicates the correctness of the ANN algorithm developed, it can also be applied for predicting the output for other input data sets.

Results and discussion

The experimental observations were made for the period of two months using each refrigerant (R22 and R433A) during the year 2016. More experimental observations were made in a DXSAHP to study the transient behavior of the system under the influence ambient conditions and also to eliminate the error-prone data. However, the performances of the system with similar ambient variations are considered for the performance comparison.

Experimental observations

The variation of ambient parameters and system operating parameters is presented in this sub section. The similar ambient conditions were observed on January 23 and

Table 3 Comparison of thermodynamic and environmental properties of refrigerants

Refrigerant	$T_b/^\circ\text{C}$	$T_{cr}/^\circ\text{C}$	P_{cr}/MPa	ODP	GWP
R22	– 40.81	96.14	4.99	0.05	1700
R290	– 42.10	96.74	4.25	0	20
R1270	– 47.70	91.06	4.55	0	20
R433A	– 44.68	94.23	4.34	0	20

Fig. 7 ANN model for exergy destruction

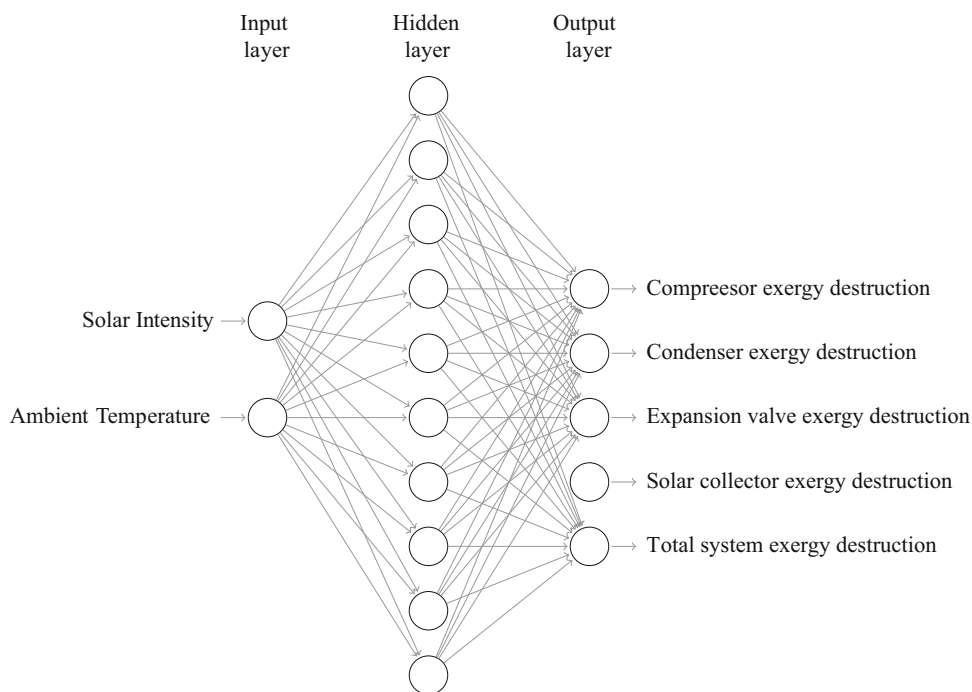
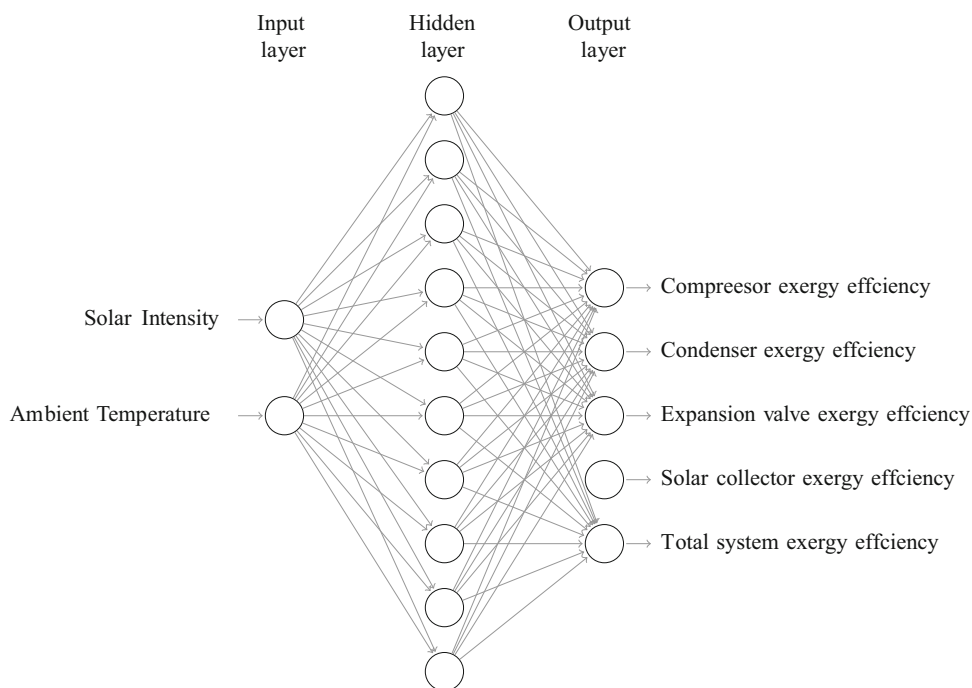


Fig. 8 ANN model for exergy efficiency



March 23, 2016, while using R22 and R433A, respectively. Hence, the experimental data are used for performance comparison.

Ambient parameters

The solar irradiation is the major influencing factor affecting the performance of DXSAHP systems. The

variations of solar irradiation during the experimentation (with R22 and R433A) are depicted in Fig. 9. It is observed that the solar irradiation that falls on the evaporator-collector has reduced the maximum value of about 950 W m^{-2} . The fluctuations in solar irradiation has observed with the $\pm 50 \text{ W m}^{-2}$ during the experimentation for both refrigerants used. Similarly, the ambient temperature variations are illustrated in Fig. 10. It is seen that the

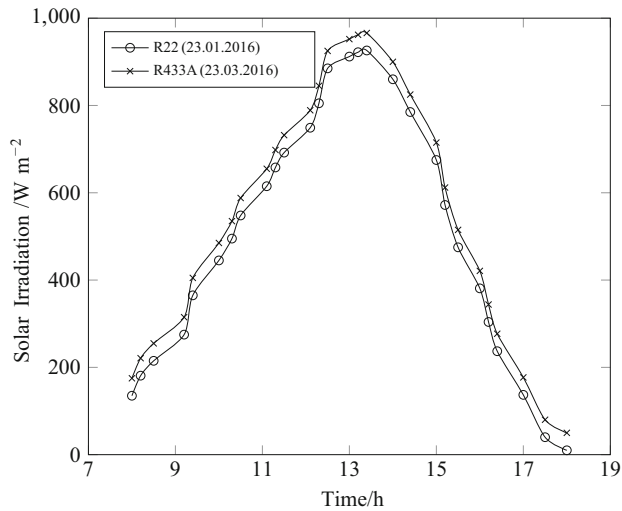


Fig. 9 Hourly variation of solar insolation during experimentation

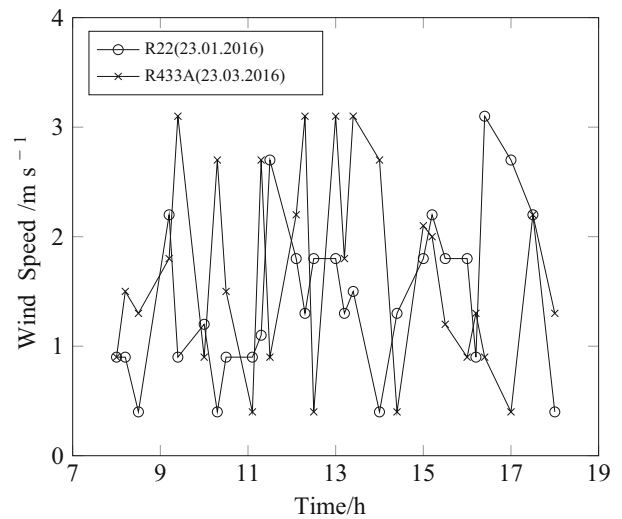


Fig. 11 Hourly variation of wind speed during experimentation

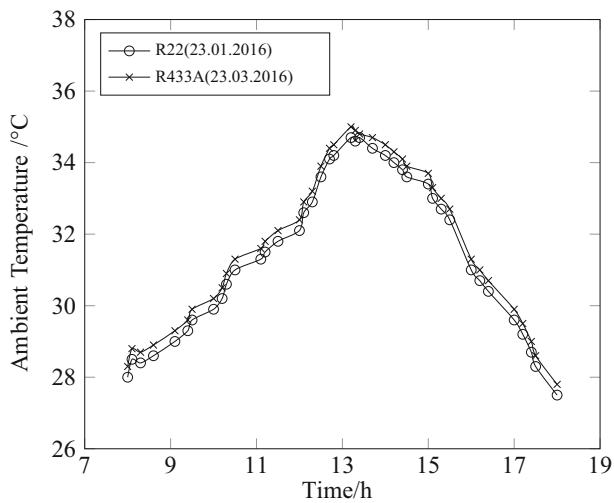


Fig. 10 Hourly variation of ambient temperature during experimentation

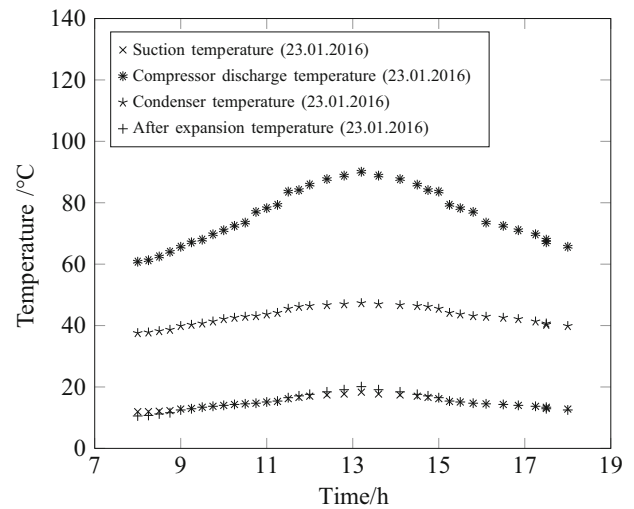


Fig. 12 Variation of temperature at different location of DXSAHP system (R22)

ambient temperature has varied from about 28 to 35 °C during the day time. The ambient wind velocity variations are shown in Fig. 11. The ambient wind velocity will influence the convective losses from the absorber plate. The convective losses from the absorber plate were reduced by placing a glazing over the absorber plate maintaining the 25 mm air gap. The temperature in the air gap gets heated due to the effect of green house effect.

System operating parameters

The refrigerant temperatures at typical locations in the refrigerant circuit of the heat pump are observed illustrated in Figs. 12 and 13, respectively, for R22 and R433A. It is observed that R22 has the average compressor inlet and outlet temperatures of 15.6 and 78.2 °C, respectively. For

expansion valve inlet and the outlet, it is about 40.2 and 15.3 °C, respectively. At similar locations for R433A, the average temperature was about 14.5 and 61.5 °C (at inlet and outlet of the compressor,) and 39.8 and 14.1 °C (at expansion valve inlet and outlet). In the above-mentioned locations, R433A represents has lower temperature when compared to the R22. This is due to the fact that hydrocarbon mixture has lower specific heat ratio (about 6.5 % less), when compared to R22. Similarly, hydrocarbon mixture has lower vapor pressure (about 3.8%) and compressor ratio (about 8.4%). Hence, lower pressure has been observed at the typical locations of the heat pump when compared to R22. The deviation of pressure at similar locations in DXSAHP system circuit for R22 and R433A working fluids is presented in Figs. 14 and 15, respectively.

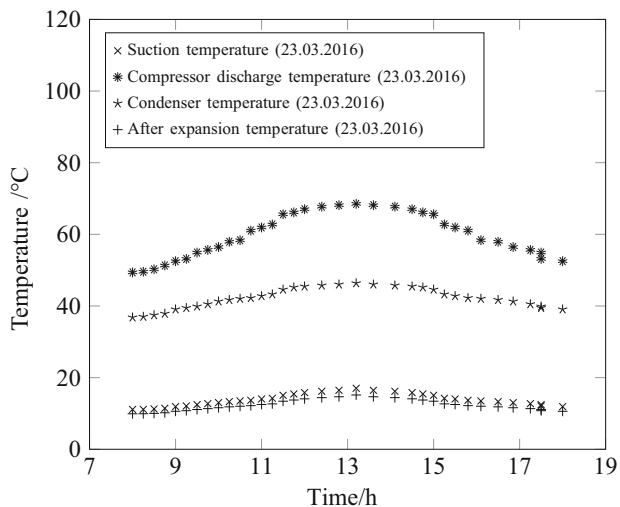


Fig. 13 Variation of temperature at different location of DXSAHP system (R433A)

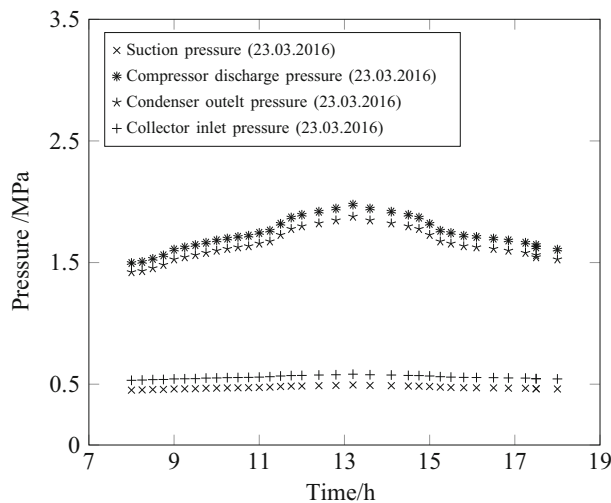


Fig. 15 Variation of pressure at different location of DXSAHP system (R433A)

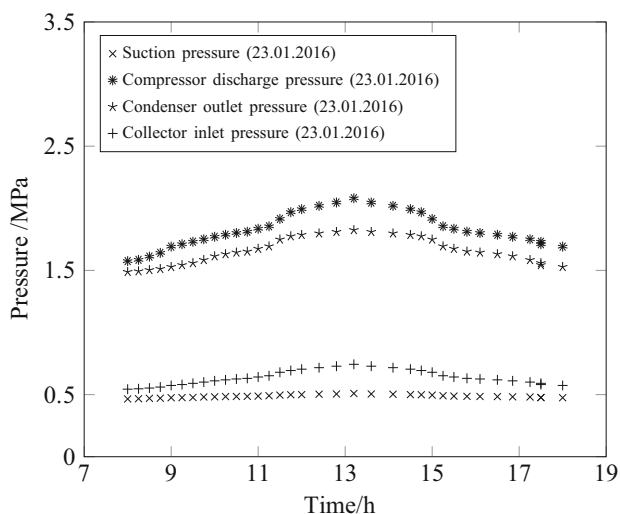


Fig. 14 Variation of pressure at different location of DXSAHP system (R22)

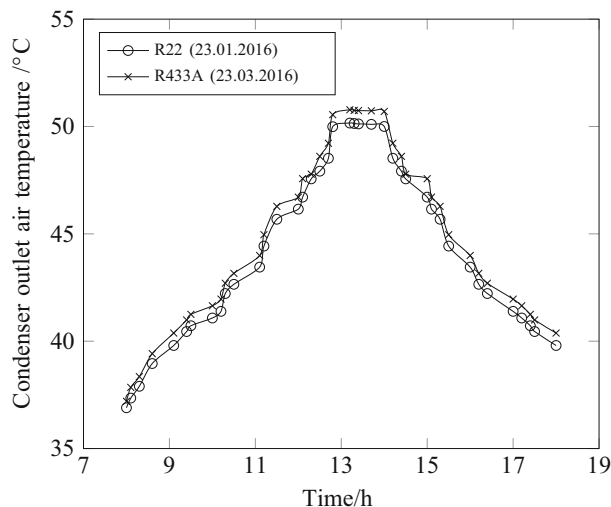


Fig. 16 Hourly variation of condenser outlet air temperature during experimentation

The average suction and discharge pressure for R22 and R433A are found to be in the range of 0.47–0.50 MPa to 1.89–2.05 MPa, respectively. The variation of condenser outlet air temperature for both refrigerants (R22 and R433A) during the experimentation is presented in Fig. 16. The condenser outlet air temperature for R433A is found to be slightly lower than that of R22. This is due to lower discharge pressure and temperature of the R433A. The average air temperature (condenser outlet) for R22 and R433A is 44.1 and 42.9 °C, respectively.

Network performance

The MLFFN configuration was optimized to 2-10-5 configuration. The statistical performance values such as R²,

COV and RMS for predicting exergy destruction and exergy efficiency of each components of the system and for the system using R22 and R433A are given in Tables 4 and 5, respectively. These results confirmed that, the ANN predicted results are closer to the experimental results with maximum fraction of absolute variance of 0.9999 for both exergy destruction and exergy efficiency of the compressor, condenser, expansion valve, evaporator–collector and total system. The root-mean-square values and coefficient of variance values found to be minimum.

Performance comparison

The exergy performance of DXSAHP system working with R22 and R433A is compared in this section.

Table 4 Performance of network for exergy destruction

	R22			R433A		
	R^2	COV	RSME	R^2	COV	RSME
Compressor	0.9987	0.6211	1.5270	0.9981	0.7938	2.0832
Condenser	0.9950	1.8855	1.7229	0.9911	1.6005	6.3987
Expansion Valve	0.9968	1.6526	3.7108	0.9913	2.3054	5.2068
Evaporator	0.9998	0.3794	1.4147	0.9991	0.5908	2.6264
Total system	0.9977	0.8386	0.0106	0.9937	1.8870	0.0265

Table 5 Performance of network for exergy efficiency

	R22			R433A		
	R^2	COV	RSME	R^2	COV	RSME
Compressor	0.9972	0.9223	0.6541	0.9960	1.7035	0.1512
Condenser	0.9929	1.6085	0.7736	0.9882	2.5927	0.2883
Expansion Valve	0.9999	0.0946	0.0842	0.9935	1.4438	0.1988
Evaporator	0.9895	2.3546	0.1769	0.9926	1.9511	0.8336
Total system	0.9864	2.0659	0.7138	0.9868	2.5335	0.8030

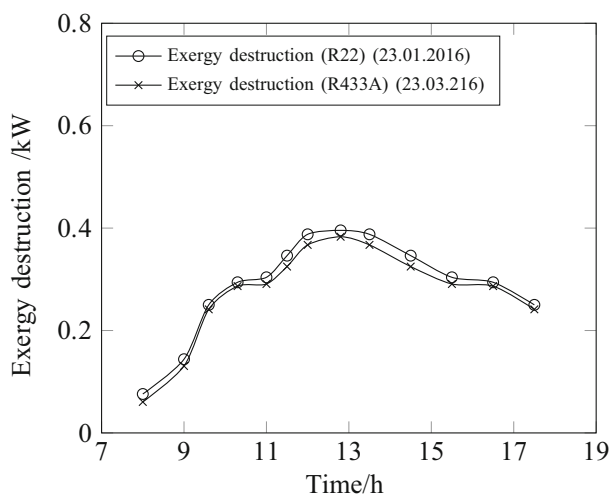


Fig. 17 Variation of exergy destruction in compressor

Compressor

The exergy destruction and exergy efficiency of the compressor used in DXSAHP system working with R22 and R433A are compared in Figs. 17 and 18, respectively. The exergy destruction of R22 and R433A has varied in the range from 0.07 to 0.36 kW with an average value of 0.25 and 0.06 kW to 0.38 kW with an average value of 0.24 kW, respectively. The average exergy destruction of R433A was found to be about 6.8% lower when compared to that of R22 due to its favorable thermo-physical properties. The lower vapor pressure of R433A (by about 3.6%) results in lower compression ratio. Hence, the exergy efficiency of

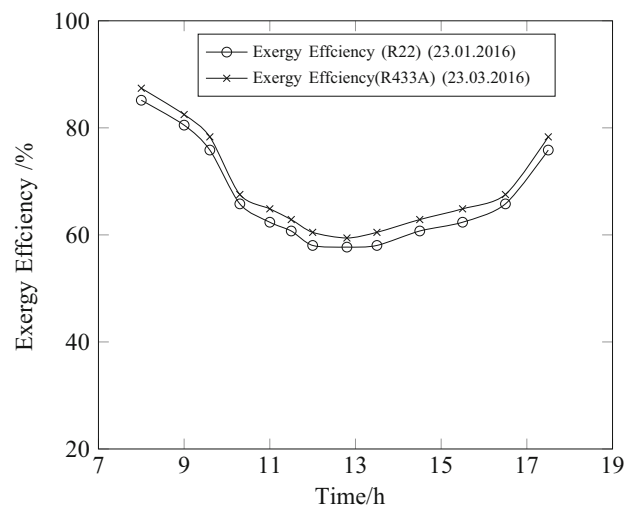


Fig. 18 Variation of exergy efficiency in compressor

compressor working with R433A is obtained as 3.2% higher than that of R22. The exergy efficiency of the compressor drops in the range between 88 and 59% for both the working fluids with an increase solar irradiation and ambient temperature. Increase in solar irradiation and ambient temperature will enhance the evaporating temperature and pressure of the working fluid. More irreversibilities will occur at higher temperature and pressure. Hence, the exergy efficiency of the compressor decreases with increase in the solar irradiation and ambient temperature. The exergy destruction in the compressor can be reduced by optimizing the compressor suction and discharge pressures.

Condenser

The variations of the exergy destruction and exergy efficiency of the condenser with reference to time of the day for R22 and R433A are shown in Figs. 19 and 20, respectively. The condenser exit temperature and outlet air temperature of condenser used in the DXSAHP system working with R433A have a lower value when compared to that of R22. Hence, lower irreversibilities are associated with R433A when compared to R22. From Fig. 19, it is observed that R433A has less exergy destruction when compared to R22. The exergy destruction of R22 was increased from 0.25 to 0.52 kW with an average value of 0.40 kW and for R433A it was increased from 0.24 to 0.51 kW with an average value of 0.39 kW. For R433A exergy

destruction value was found to be about 3.7% lower when compared to that of R22 (due to its temperature glide of 0.5 °C). Similarly, the condenser exergy efficiency of DXSAHP system working with R22 and R433A was increased from about 38–61%. The exergy efficiency of the condenser working with R433A was found to be higher in the range of 2.8–4.2% when compared to that of R22. The exergy analysis of the condenser helps to optimize the air mass flow rate passing over the condenser tubes.

Expansion valve

The variations of exergy destruction and exergy efficiency of a thermostatic expansion valve, used in the DXSAHP system working with R22 and R433A, are depicted in Figs. 21 and 22, respectively. In general, the evaporator

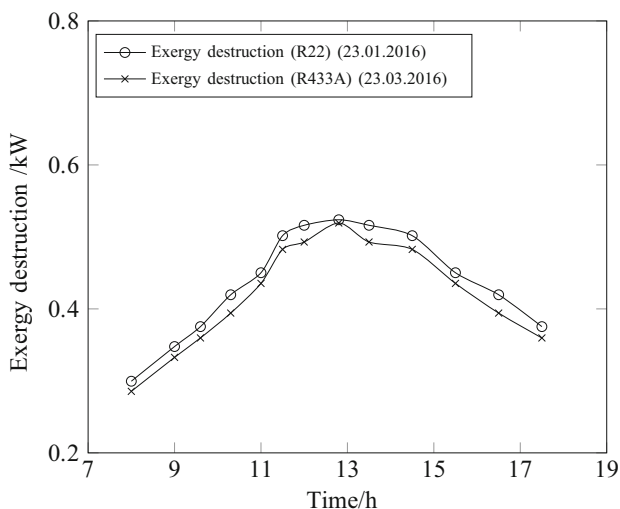


Fig. 19 Variation of exergy destruction in condenser

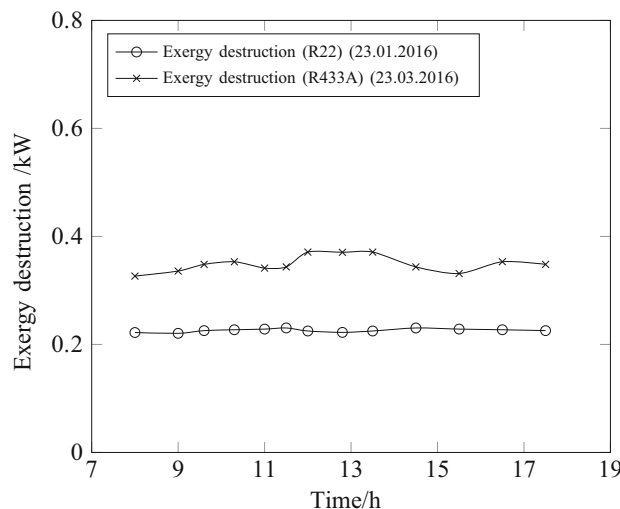


Fig. 21 Variation of exergy destruction in expansion valve

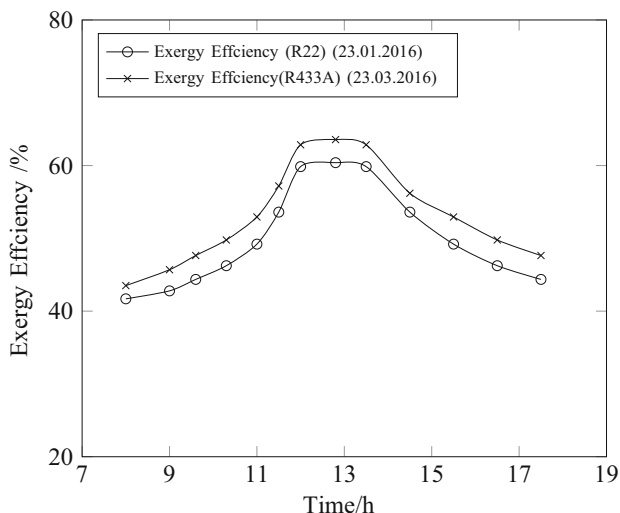


Fig. 20 Variation of exergy efficiency in condenser

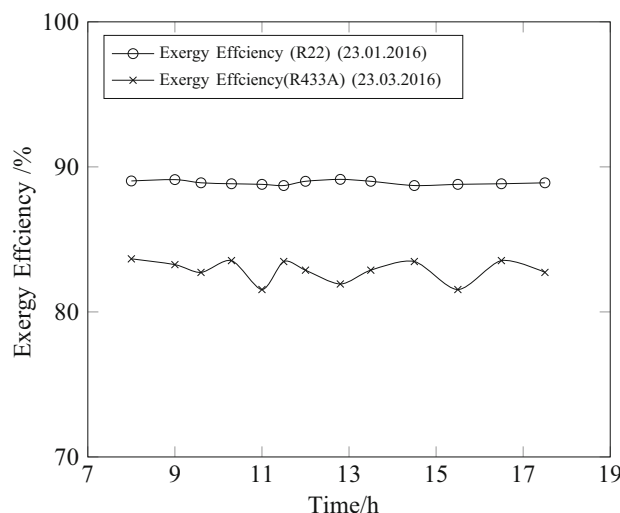


Fig. 22 Variation of exergy efficiency in expansion valve

load fluctuates due to the variation in solar irradiation and ambient temperature. This will cause pressure differences in the expansion valve, which influence the irreversibilities in the system. It is observed that the variation of exergy destruction for R22 has found to in the range between 0.21 and 0.22 kW with an average value of 0.23 kW. Similarly, for R433A is in the range between 0.31 and 0.37 kW with an average value of 0.34 kW. Higher exergy destruction of R433A was observed as compared to R22. The average exergy efficiency values of a thermostatic expansion valve used in the DXSAHP system working with R22 and R433A were calculated as 88 and 83%, respectively. The exergy efficiency of R22 was found to be slightly higher when compared to that of R433A. The exergy destruction associated with an expansion valve has found to be very small (for both refrigerants). It can be further reduced by using electronic expansion valve, which controls the refrigerant mass flow rate automatically.

Evaporator–collector

The comparison of exergy destruction and exergy efficiency of the solar collector (which acts as the evaporator of the system) used in the DXSAHP system (working with R22 and R433A) is presented in Figs. 23 and 24, respectively. The exergy destruction of evaporator–collector working with R22 was found to be in the range between 0.43 and 0.52 kW with an average value of 0.48 kW. Similarly, for R433A it was found that in the range between 0.23 and 0.32 kW with an average value of 0.28 kW. The R433A has lower exergy destruction when compared to R22. This is due to its higher latent heat. The higher latent heat of R433A can absorb more heat and reduce the losses when compared to R22. The exergy

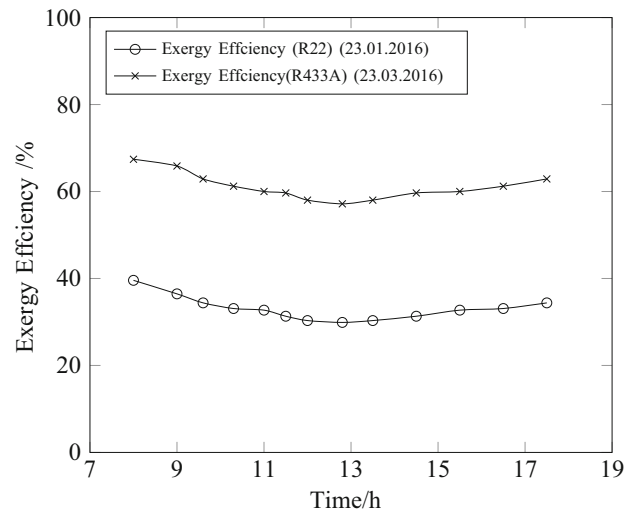


Fig. 24 Variation of exergy efficiency in collector–evaporator

efficiencies of R22 and R433A have dropped from 41 to 29 and from 66 to 57%, respectively.

Total system

The variations of exergy destruction and exergy efficiencies of the DXSAHP system working with R22 and R433A are compared in Figs. 25 and 26, respectively. An increase in solar irradiation and ambient temperature will lead higher refrigerant temperature and pressure, which influences the exergy destruction. The exergy destruction of system working with R22 varied from 0.92 to 1.66 kW with an average value of 1.36 kW. Similarly, for R433A varied from 0.81 to 1.62 kW with an average value of 1.25 kW, respectively. The exergy destruction of R433A was found to be 8.75% lower when compared to that of R22.

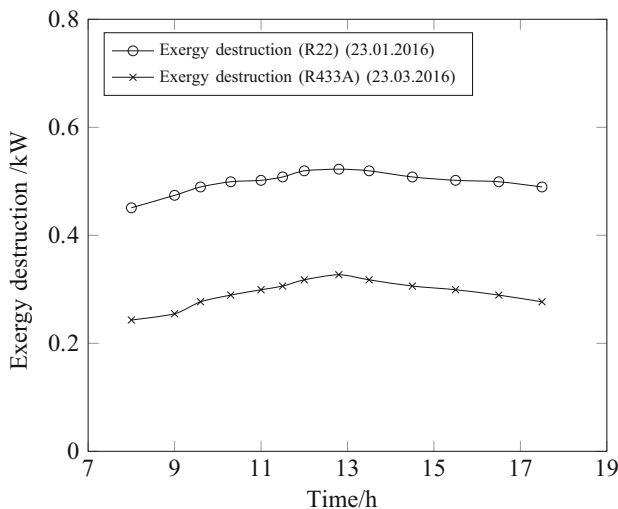


Fig. 23 Variation of exergy destruction in collector–evaporator

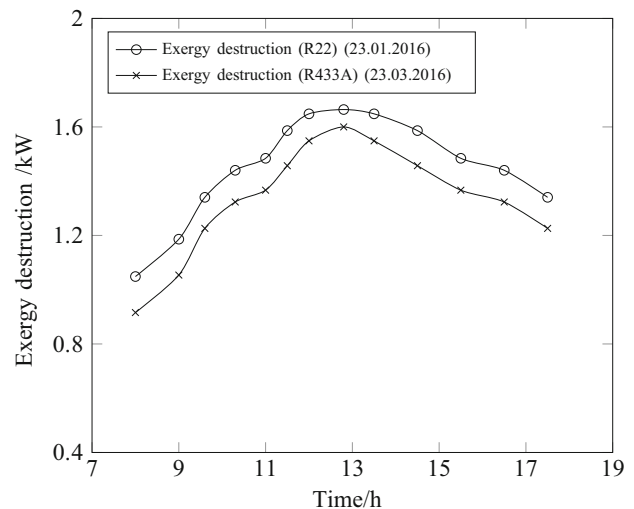


Fig. 25 Variation of exergy destruction of a total system

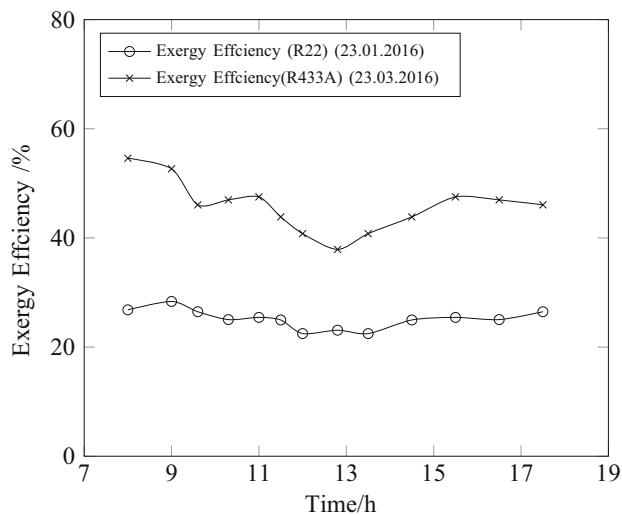


Fig. 26 Variation of exergy efficiency of a total system

The exergy efficiency of the system has dropped from 33 to 23% for R22 and for R433A 58 to 37%, respectively. Higher exergy efficiency is observed for both working fluids when solar irradiation is in the range between 400 and 600 W m⁻². The exergy assessment results of a DXSAHP system working with R22 are similar to the results of earlier studies reported by Mohanraj et al. [13].

Conclusions

The exergy performance of a DXSAHP system using R22 and R433A was assessed for the climatic conditions of Calicut, during the year 2016. The following major conclusions are drawn;

- The MLFFN with 2-10-5 predicts the exergy destruction and exergy efficiency with maximum fraction of absolute variance, minimum RMS and COV values.
- The maximum exergy destruction was occurred evaporator–collector followed by condenser, compressor and expansion valve when system was working with R22. For R433A maximum exergy destruction was observed in condenser followed by expansion valve, collector–evaporator and compressor.
- The exergy destruction of compressor, condenser, expansion valve and evaporator–collector for R22 is 0.25, 0.40, 0.23 and 0.48 kW, respectively. Similarly, exergy destruction of compressor, condenser, expansion valve and evaporator–collector is 0.24, 0.39, 0.34 and 0.28 kW, respectively, for R433A.
- The average exergy destruction of the system using R22 and R433A is found to be 1.36 and 1.25 kW, respectively.

The results confirmed that R433A is a good environment-friendly and energy-efficient alternative refrigerant to phase out R22 in solar heat pump applications. However, the operating parameters of the condenser need to be optimized to reduce the exergy destructions when the system is retrofitted with R433A.

References

1. Mohanraj M, Belyayev Y, Jayaraj S, Kaltayev A. Research and developments on solar assisted compression heat pump systems—a comprehensive review (Part A: modeling and modifications). *Renew Sustain Energy Rev.* 2018;83:90–123.
2. Hawlader M, Jahangeer K. Solar heat pump drying and water heating in the tropics. *Sol Energy.* 2006;80(5):492–9.
3. Li Y, Wang R, Wu J, Xu Y. Experimental performance analysis on a direct expansion solar-assisted heat pump water heater. *Appl Therm Eng.* 2007;27:2858–68.
4. Mohanraj M, Belyayev Y, Jayaraj S, Kaltayev A. Research and developments on solar assisted compression heat pump systems—a comprehensive review (Part A: modeling and modifications). *Renew Sustain Energy Rev.* 2018;83:124–55.
5. Ozgener O, Hepbasli A. Modeling and performance evaluation of ground source (geothermal) heat pump systems. *Energy Build.* 2007;39(1):66–75.
6. Ozgener O, Hepbasli A. Performance analysis of a solar-assisted ground-source heat pump system for greenhouse heating: an experimental study. *Build Environ.* 2005;40(8):1040–50.
7. Ozgener O, Hepbasli A. Experimental investigation of the performance of a solar-assisted ground-source heat pump system for greenhouse heating. *Int J Energy Res.* 2005;29(3):217–31.
8. Mohanraj M, Muraleedharan C, Jayaraj S. A review on recent developments in new refrigerant mixtures for vapour compression-based refrigeration, air-conditioning and heat pump units. *Int J Energy Res.* 2011;35(8):647–69.
9. Mohanraj M, Muraleedharan C, Jayaraj S. Environment friendly alternatives to halogenated refrigerants—a review. *Int J Greenhouse Gas Control.* 2009;3(1):108–19.
10. Chata FG, Chaturvedi S, Almogbel A. Analysis of a direct expansion solar assisted heat pump using different refrigerants. *Energy Convers Manag.* 2005;46:2614–24.
11. Chaichana C, Aye L, Charters W. Natural working fluids for solar-boosted heat pumps. *Int J Refrig.* 2003;26(6):637–43.
12. Mohanraj M, Muraleedharan C, Jayaraj S. A comparison of the performance of a direct expansion solar-assisted heat pump working with R22 and R407C/liquid petroleum gas. *Proc Inst Mech Eng Part A J Power Energy.* 2009;223:821.
13. Mohanraj M, Jayaraj S, Muraleedharan C. Exergy assessment of a direct expansion solar-assisted heat pump working with R22 and R407C/LPG mixture. *Int J Green Energy.* 2010;65(83):65–83.
14. Hepbasli A. Exergetic modeling and assessment of solar assisted domestic hot water tank integrated ground-source heat pump systems for residences. *Energy Build.* 2007;39(12):1211–7.
15. Dikici A, Akbulut A. Performance characteristics and energy-exergy analysis of solar-assisted heat pump system. *Build Environ.* 2008;43(11):1961–72.
16. Dikici A, Akbulut A. Exergetic performance evaluation of heat pump systems having various heat sources. *Int J Energy Res.* 2008;32(14):1279–96.
17. Ozgener O, Hepbasli A. A parametrical study on the energetic and exergetic assessment of a solar-assisted vertical ground-

- source heat pump system used for heating a greenhouse. *Build Environ.* 2007;42(1):11–24.
18. Ozgener O, Hepbasli A. Experimental performance analysis of a solar assisted ground-source heat pump greenhouse heating system. *Energy Build.* 2005;37(1):101–10.
 19. Torres-Reyes E, Cervantes de Gortari J. Optimal performance of an irreversible solar-assisted heat pump. *Exergy Int J.* 2001;1(2):107–11.
 20. Mohanraj M, Muraleedharan C, Jayaraj S. Exergy analysis of direct expansion solar-assisted heat pumps using artificial neural networks. *Int J Energy Res.* 2009;33(11):1005–20.
 21. Kara O, Ulgen K, Hepbasli A. Exergetic assessment of direct-expansion solar-assisted heat pump systems: review and modeling. *Renew Sustain Energy Rev.* 2008;12(5):1383–401.
 22. Torres RE, Picon Nuez M, de Cervantes GJ. Exergy analysis and optimization of a solar-assisted heat pump. *Energy.* 1998;23(4):337–44.
 23. Cervantes GJ, Torres-Reyes E. Experiments on a solar-assisted heat pump and an exergy analysis of the system. *Appl Therm Eng.* 2002;22(12):1289–97.
 24. Mohanraj M, Jayaraj S, Muraleedharan C. Applications of artificial neural networks for refrigeration, air-conditioning and heat pump systems—a review. *Renew Sustain Energy Rev.* 2012;16(2):1340–58.
 25. Kalogirou SA. Applications of artificial neural-networks for energy systems. *Appl Energy.* 2000;67(2):17–35.
 26. Mohanraj M, Jayaraj S, Muraleedharan C. Applications of artificial neural networks for thermal analysis of heat exchangers—a review. *Int J Therm Sci.* 2015;90:150–72.
 27. Mohanraj M, Muraleedharan C, Jayaraj S. Performance prediction of a direct expansion solar assisted heat pump using artificial neural networks. *Appl Energy.* 2009;86:1442–9.
 28. Esen H, Inalli M, Sengur A, Esen M. Performance prediction of a ground-coupled heat pump system using artificial neural networks. *Expert Syst Appl.* 2008;35(4):1940–8.
 29. Gunasekar N, Mohanraj M, Velumuragan V. Artificial neural network modelling of a photovoltaic-thermal evaporator for solar assisted heat pumps. *Energy.* 2015;91:255–64.
 30. Shariah A, Al-Akhras M, Al-Omar A. Optimizing the tilt angle of solar collectors. *Renew Energy.* 2002;26:587–98.
 31. Bechtler H, Browne MW, Bansal PK, Kecman V. Neural networks a new approach to model vapour-compression heat pumps. *Int J Energy Res.* 2001;25(7):591–9.